Final Draft
of the original manuscript:

Yi, S.; Brokmeier, H.-G.; Letzig, D.**:**

Microstructural evolution during the annealing of an extruded AZ31 magnesium alloy

Microstructural evolution during the annealing of an extruded AZ31 magnesium alloy

Sangbong Yi[1*], Heinz-Günter Brokmeier[1,2], Dietmar Letzig[1]

[1] Magnesium Innovation Centre, GKSS-Research Centre, Max-Planck-Str., D-21502, Geesthacht, Germany

[2] Institute of Materials Science and Engineering, Clausthal University of Technology, Agricolastr. 6, D-38678, Clausthal-Zellerfeld, Germany

Abstract

Microstructural evolution during the annealing of AZ31 extruded rod at 400 °C has been examined by employing neutron diffraction and electron backscatter diffraction (EBSD). In the as-extruded bar, equiaxed grains smaller than 5 µm and large elongated grains having significant degrees of internal misorientation are oriented mainly with $<10\bar{1}0>$ parallel to the extrusion direction. Rapid grain growth occurs within the 180 sec annealing period at 400 °C at the expense of the small grains with the internal orientation gradient as driving force. After short time annealing, small equiaxed grains are formed inside the large elongated grains, and grains having $<11\bar{2}0>$ parallel to the extrusion direction show preferred growth. As a result, a transition of the main texture component to the $<11\bar{2}0>$ component occurs after annealing for 1800 sec at 400 °C.

Keywords; Magnesium alloy, Extrusion, Microstructure, Grain growth, Texture, AZ31

Corresponding author:

S.B. Yi (sangbong.yi@gkss.de)

Magnesium Innovation Centre, GKSS Research Centre, Max-Planck-Str. 1, D-21502, Geesthacht, Germany

Tel) +49-(0)4152-871911, Fax) +49-(0)4152-871927

1. Introduction

The processing of wrought Mg alloys is conducted mostly at elevated temperatures due to limited room temperature formability. In order to improve the properties of wrought products, it is therefore important to understand the dynamic variation of the microstructure during hot forming processes. Extensive research has been carried out on dynamic recrystallisation (DRX). It is well known that new grains are formed mainly by discontinuous (DDRX) or rotational dynamic recrystallisation (RDRX) [1-7]. In DDRX, new grains are formed usually by boundary bulging, for example, via strain induced boundary migration. On the other hand, RDRX is associated with the development of new high angle boundaries by progressive lattice rotation as a result of dislocation accumulation that is promoted by intergranular strain incompatibility. DDRXed grains are thus expected to be relatively strain-free, while RDRXed grains should show high dislocation densities.

The microstructural features of warm extruded Mg-Al-Zn (AZ series) alloys, e.g. the sizes of the DRXed grains and the degree of recrystallisation, are strongly dependent on the extrusion parameters and alloy compositions [8-10]. A microstructure more characteristic of the deformed state is generally present after hydrostatic extrusion, as the increase in temperature caused by friction is smaller during hydrostatic extrusion compared to direct or indirect extrusion [11]. The size of DRXed grains increases with increasing processing temperature [9] and extrusion ratio [12]. Chen et al. [13] observed, however, grain refinement in AZ31 with increasing extrusion ratio and Swiostek et al. [14] reported that increasing the Al content resulted in grain coarsening after hydrostatic extrusion.

Alloying additions of rare earth (RE) elements generally result in significant texture weakening [15, 16]. In RE-free Mg alloys various textures can be formed depending on the extrusion parameters. Although a fibre-type texture in which the $<10\bar{1}0>$ directions of the crystallites align parallel to the ED is mostly observed in extruded rods, the $<11\bar{2}0>$-fibre and the $<10\bar{1}0>$ - $<11\bar{2}0>$ double fibre texture parallel to the ED are also often observed [10, 15, 17-20]. Nevertheless, it is widely unknown which mechanisms are responsible for these texture variations and their relation with the microstructure.

The present work examines microstructural evolution in a hydrostatically extruded AZ31 rod during post-extrusion annealing at 400 °C. The partially DRXed grain structure in the as-extruded rod thus allows microstructural evolution during subsequent static recrystallisation to be investigated. Besides analysing the microstructural evolution during annealing treatments, the present study also aims to provide a way of understanding the formation mechanism of various textures and microstructures in extruded Mg alloys. Although the microstructure and texture developed during extrusion originate from dynamic processes such as DRX should be interpreted differently to those resulting from the static recrystallisation process, microstructural evolution during annealing treatments can be related to that found in an as-extruded material for the following reasons. Firstly, microstructural evolution by DDRX is comparable to static recrystallisation. Secondly, an extruded profile experiences a procedure similar to an annealing treatment during air cooling at the extrusion die exit. In fact, significant grain growth has been observed during air cooling after exit from the extrusion die [21]. The degree of annealing during cooling can be controlled relatively easily by the choice of feedstock temperature, extrusion speed and profile dimensions. Moreover, the cooling rate after extrusion is dependent on the profile dimensions and cooling method. Therefore, an understanding of microstructural evolution during annealing treatments is essential in order to analyse the diversity of textures and microstructures as well as to optimise the extrusion parameters.

2. Experimental procedures

The starting material was a round AZ31 rod (Mg - 3Al – 1Zn – 0.3 Mn in wt. %) with 15 mm diameter, which was hydrostatically extruded at 300 °C with an extrusion ratio of 14 : 1. The extruded profile was water-cooled 80 cm behind the die exit to avoid annealing during cooling. Samples with a length of 15 mm were prepared from the extruded rod for post-extrusion annealing. Annealing treatments were conducted at 400 °C for various holding times of 180, 300, 600, 900 and 1800 sec and samples were subsequently water quenched. Because the profile temperature during extrusion processing generally reaches 300 ~ 450 °C, depending on the extrusion method and speed, an annealing temperature of 400 °C was applied in the present study. Microstructural evolution comparable to that seen following extrusion (e.g. the occurrence of DDRX and / or effects due to cooling after exit from the die) can be obtained.

Global texture measurements were carried out using the TEX-2 neutron diffractometer at the GKSS-Research Centre in Germany [22]. Using the 4 measured pole figures, $\{10\bar{1}0\}$, (0002), $\{10\bar{1}1\}$ and $\{11\bar{2}0\}$, inverse pole figures were calculated by the iterative series expansion method. Samples for electron backscatter diffraction (EBSD) measurements were prepared by electro-chemical polishing (using the Struers AC2 solution for 100 sec at 18 V and about 0 °C) following mechanical polishing down to 1 µm with alumina powder. The EBSD measurements were conducted with a 0.2 µm step size on longitudinal sections cut from the mid-plane of the extruded rod.

3. Results and discussion

The textures of the as-extruded and annealed samples after different annealing times at 400 °C, in terms of inverse pole figures in the ED calculated using neutron diffraction data, are displayed in Fig. 1. The extruded bar shows a strong $<10\bar{1}0>$ fibre texture. Extrusion

involves deformation similar to uni-axial loading such that the basal planes, which contain the $<11\bar{2}0>$ Burgers vectors of the dislocations mainly activated, are rotated to be parallel to the main deformation axis (ED). The formation of this texture type has been observed in round extruded magnesium alloys [10, 17, 21] as well as in other hexagonal metals, e.g. Ti [23], Zr [24] and Be [25]. With increasing annealing time at 400 °C, the $<10\bar{1}0>$-fibre component is observed to weaken and the intensity on the inverse pole figure becomes more homogeneously distributed between the $<10\bar{1}0>$ and $<11\bar{2}0>$ poles. The $<11\bar{2}0>$-fibre component becomes visible after 300 sec annealing. As can also be seen from the pole density variation with annealing time in Fig. 2, the $<11\bar{2}0>$ component strengthens gradually at the expense of the $<10\bar{1}0>$ component and becomes the main texture component after 1800 sec. The present results show that various texture types are produced depending on the annealing time, i.e. on the degree of recrystallisation / grain growth. In order to investigate the variations in microstructure and texture during annealing in more detail, EBSD measurements of the as-extruded and annealed samples were carried out.

An EBSD orientation map of the as-extruded AZ31 rod is presented in Fig. 3, as an inverse pole figure map in the ED. The microstructure consists of equiaxed grains with an average size of 4.1 µm and large grains elongated in the ED with lengths of some hundreds of microns. In the present study, equiaxed grains were defined as grains having a grain aspect ratio (the length of the minor axis / the length of the major axis) larger than 0.3. The equiaxed grains are formed by DRX, while the elongated grains represent the deformed state of the initial microstructure of the feedstock for the extrusion [21]. The orientations of 36 large elongated grains in the as-extruded as well as in the heat treated rods were examined in the present study. All show an orientation of $<10\bar{1}0>$ parallel to the ED without exception. This corresponds to the $<10\bar{1}0>$ fibre texture component of the extruded rod. The internal misorientation within the large elongated grains, which is visible as colour gradients within the grains, indicates that

they have maintained their deformed status. Fig. 3 (b) shows a magnified view of the area marked in the Fig. 3 (a). High angle boundaries (HAGB, with misorientation angles larger than 12 °) are marked in black and low angle boundaries (LAGB, with misorientation angles smaller than 12 °) are grey. The formation of LAGBs is clearly visible in the vicinity of the boundaries of the equiaxed grains, as well as in the elongated grains, especially in grains with the $<10\bar{1}0>$ fibre texture component. These are marked with black arrows in Fig. 3 (b). New grains with HAGBs are also formed in several areas near to the boundaries of the matrix grains, marked as white circles in Fig. 3 (b), and these are not strain-free. Large internal misorientations are indicated by the large kernel average misorientations in Fig. 5 (a). Moreover, they show no large deviations in orientation with respect to the matrix grain. These microstructural characteristics correspond to the RDRX mechanism [1, 3].

The fine equiaxed microstructure (< 5 µm) in the as-extruded rod can be classified into grains with and without internal misorientations. The fraction of fine strain-free grains, defined as grains having internal orientation spreads < 0.5 °, is significantly smaller than that having internal misorienations > 0.5 °. The former has an area fraction, f, of 0.06, and the latter 0.56. The formation of the fine strain-free grains in the as-extruded rod can be explained by the DDRX mechanism, while the appearance of the large fraction of fine grains having internal misorientations can be understood to be a result of RDRX or as an indication of the deformed status of DDRXed grains. The inverse pole figures evaluated from these grain classes are presented in Fig. 3 (c). The $<10\bar{1}0>$-fibre component is observed in both, although in the grains having internal misorientations a slightly higher intensity of the $<10\bar{1}0>$ component is revealed. In contrast to the fine equiaxed grains, no internal misorientations are observed in the relatively large grains (> 10 µm). Moreover, the inverse pole figure evaluated from the large equiaxed grains shows the $<10\bar{1}0>$ as well as the $<11\bar{2}0>$ texture components.

An EBSD orientation map of a sample annealed for 180 sec at 400 °C is presented in Fig. 4. Rapid growth of the equiaxed grains occurred during annealing and their average grain size

reached 20.6 µm, while the large elongated grains maintained their shapes and sizes. When comparing the area fractions of the equiaxed grains having $<10\bar{1}0>$ and $<11\bar{2}0>$ fibre components in the as-extruded sample ($f_{<10\bar{1}0>}$ = 0.33 with average grain size of 3.5 µm, $f_{<11\bar{2}0>}$ = 0.14 with 3.9 µm) with those in the sample annealed for 180 sec ($f_{<10\bar{1}0>}$ = 0.16 with 15.4 µm, $f_{<11\bar{2}0>}$ = 0.32 with 26.1 µm), it is clear that the grains having a $<11\bar{2}0>$ orientation grew more effectively than those with a $<10\bar{1}0>$ component. Area fractions were calculated by considering grains having angular deviations within 15 ° of the $<10\bar{1}0>$ and $<11\bar{2}0>$ fibre components, respectively. The large internal misorientations in the fine equiaxed grains in the as-extruded condition and the small grain size are thought to provide the driving force for rapid grain growth. Interestingly, the formation of some small grains is observed within the large elongated grains, Fig. 4 (a). These grains, with sizes between 1 and 5 µm, are not present in the as-extruded rod. The misorientation profiles (point to origin) along the lines marked in the orientation map are displayed in Fig. 4 (b). The degree of misorientation in the longitudinal direction of the large elongated grain (profile 'a', max misorientation degree = 4.5 ° within 50 µm), i.e. along the ED, is much smaller compared to that along the direction perpendicular to the ED (profile 'b', max degree of misorientation = 26 ° within 12 µm). The orientation gradient within the large elongated grain retains the $<1\bar{1}00>$ // ED component, as presented in the orientation trace along the lines 'a' and 'b' on the $\{10\bar{1}0\}$ pole figure, Fig. 4 (b). For example, the misorientation relation between two points in the elongated grain, 'A' and 'B', can be described as a rotation of 26.5° around the $<1\bar{1}00>$ axis. The development of band-shaped agglomerates of small equiaxed grains within the large elongated grain is observed when a large degree of misorientation exists. Although the elongated grain seems to be divided by the band of small equiaxed ones into two grains, it is believed to be a single grain because of the gradual increase in the misorientation (profile 'a') and the image contrast in the upper part of Fig. 4 (a). In all areas inside the elongated grains where fine equiaxed

grains appear, large degrees of internal misorientation are found. The orientations of the fine grains developed within an elongated grain are presented in Fig. 4 (c), in terms of the inverse pole figures evaluated separately from grains smaller and larger than 3 μm. It is to be noted that the inverse pole figures in Fig. 4 (c) are meaningful only for qualitative analysis as a result of the poor grain statistics. Grains smaller than 3 μm have mainly $<10\bar{1}0>$ // ED orientations, which are similar to the orientation of the elongated grains. Larger grains (> 3 μm) have mainly $<11\bar{2}0>$ // ED orientations. This result indicates that grain growth is accompanied by a gradual orientation change from a $<10\bar{1}0>$ to a $<11\bar{2}0>$ fibre texture.

Fig. 5 presents EBSD kernel average misorientation (KAM) maps of the as-extruded rod and the sample annealed for 180 sec. The KAM maps are constructed on the basis of the degree of misorientation between a measuring point (kernel) and all its surrounding neighbours, such that the local misorientation and the degree of strain energy can be clearly represented. The present study used the 3rd neighbours for defining a kernel, i.e. the local degree of misorientation within 0.6 μm is plotted in Fig. 5. The as-extruded sample shows large local misorientations in the large elongated grains as well as in the equiaxed grains. In contrast, the equiaxed grains in the sample annealed for 180 sec show mostly a misorientation-free status, while the large elongated grains still possess relatively large local degrees of misorientation. Fig. 5 (c) shows the area fraction of the equiaxed grains having kernel average misorientations larger than 2 ° as a function of the annealing time. The rapid decrease in the area fraction of grains with large internal misorientations, i.e. those with high strain energy, is clearly shown after 180 sec annealing at 400 °C. This result confirms that the local degree of misorientation is one of the important driving forces for grain growth. Since the stored strain energy is mostly exhausted already after 180 sec annealing, it can be assumed that further grain growth will be less rapid.

The EBSD orientation maps of the samples annealed for 600 sec and 1800 sec at 400 °C are displayed in Fig. 6. The large elongated grains are still visible in the sample annealed for 600

sec. The fraction of equiaxed grains increases gradually with annealing time and the sample annealed for 1800 sec is dominated by equiaxed grains with an area fraction of 0.95. The area fractions of the equiaxed grains having the $<10\overline{1}0>$ and $<11\overline{2}0>$ components show slight variations with annealing time, e.g. a decrease in the former and an increase in the latter ($f_{<10\overline{1}0>}$ = 0.16, $f_{<11\overline{2}0>}$ = 0.35 and $f_{<10\overline{1}0>}$ = 0.15, $f_{<11\overline{2}0>}$ = 0.40 in the samples annealed for 600 sec and 1800 sec, respectively). Grains with both orientations undergo growth during annealing, however, the grains having the $<11\overline{2}0>$ component show more effective growth than those having the $<10\overline{1}0>$ component. As shown in Table 1, the average grain size of the former is about 10 µm larger than the latter in all annealed samples.

Similar to the sample annealed for 180 sec, the development of fine equiaxed grains within large elongated ones is also observed in the sample annealed for 600 sec in which relatively large internal degrees of misorientation exist, marked as black arrows in Fig. 6 (a). The smaller fraction of fine equiaxed grains (< 3µm) within the large elongated ones compared to the sample annealed for 180 sec can be understood as a result of grain growth in the band-shaped agglomerates during annealing. Actually, a group of grains with average grain size of 24 µm (marked by a dashed rectangle) is observed between the long elongated grains in Fig. 6 (a). The orientation relationship between the large elongated grains (A* and B*) adjacent to the band-shaped agglomerates marked is found to be approximately 20 ° about the $<10\overline{1}0>$ axis, which is similar to that between the areas A and B in the sample annealed for 180 sec. The orientation of the band-shaped agglomerates of equiaxed grains is also illustrated in Fig. 6 (c). A comparison with the inverse pole figures shown in Fig. 4 (c) reveals that the transition of the main texture component to the $<11\overline{2}0>$ fibre orientation occurs during grain growth, even in the grains formed by the static annealing process. The shapes of most grains growing between the elongated ones are actually not fully equiaxed but rectangular / oval forms with their long axes along the ED. Because the large elongated grains are stable as a result of their large volumes, the growth of the grains within the band-shaped agglomerates is considerably

retarded in the direction perpendicular to the ED, even though the internal degrees of misorientation in the elongated grains are much larger in this direction than in the ED. Subsequently, rectangular / oval shaped grains appear along the band-shaped aggregates.

During annealing for 1800 sec at 400 °C, the equiaxed grains grow into the long elongated ones such that equiaxed grains become dominant. Moreover, it can be deduced from the above results that the large elongated grains can be divided more easily into small equiaxed grains when larger degrees of internal misorientation exist. This can be controlled in principle by the choice of extrusion ratio and process temperature.

Variations in the grain size distribution and the area fraction of equiaxed grains are summarised in Table 1 and Fig. 7. Table 1 shows the area fractions of equiaxed grains smaller than 5 µm and larger than 40 µm as well as the grains having the $<10\bar{1}0>$ and $<11\bar{2}0>$ components, without considering the large elongated ones. Although the decrease in the area fraction of elongated grains during annealing is obvious, its variation has not been considered in the present study, because the initial sizes and area fractions are different in each sample and this would cause inaccuracy from a statistical viewpoint. The significant changes in the area fractions of the equiaxed grains in different size ranges takes place basically within a short annealing treatment. For example, the area fraction of the small grains (< 5 µm) changes from $f = 0.62$ in the as-extruded to $f = 0.11$ in the sample annealed for 180 sec, and that of the large grains (> 40 µm) from $f = 0$ to $f = 0.19$. Further annealing causes gradual changes in the grain sizes, but only to a small extent. Similar to the variation in the grain size, the area fractions of the grains with $<10\bar{1}0>$ and $<11\bar{2}0>$ components show remarkable changes within the annealing time of 180 sec. Thereafter, the fraction of grains having the $<11\bar{2}0>$ component increases slightly with annealing time, while the fraction having the $<10\bar{1}0>$ orientation decreases. The inverse pole figures evaluated from the equiaxed grains larger than 40 µm in the samples annealed for 180, 600 and 1800 sec are presented in Fig. 8. Since the average sizes of the equiaxed grains in the annealed samples are smaller than 40 µm, the

inverse pole figures in Fig. 8 represent the orientations of the grains that grow preferentially

during annealing. A strong $<11\bar{2}0>$-fibre component is observed in all the annealed samples.

This result verifies that the transition of the main texture component during annealing is

caused by the preferential growth of grains having the $<11\bar{2}0>$ component.

The texture transition from the $<10\bar{1}0>$ to the $<11\bar{2}0>$ component as well as the preferential

growth of grains having the $<11\bar{2}0>$ texture component suggests that boundaries having a

30 ° misorientation around the c-axes have a high mobility, a feature which has been reported

in studies on the recrystallisation behaviour of metals with hexagonal structure [26]. It should

be noted, however, that only very few boundaries with this special misorientation relationship

were observed in the samples investigated in the present study (about 0.01 of the number

fraction), while boundaries having a 30 ° ± 5° misorientation angle around randomly selected

rotation axes are mostly found in the annealed samples (about 0.12 ~ 0.16 of the number

fraction of all boundaries found in a sample).

4. Summary

Microstructural evolution in hydrostatically extruded AZ31 rod during annealing at 400 °C

has been examined in the present study. The results show that grain growth in the early stages

of annealing is facilitated by the large fraction of small grains in the as-extruded condition, i.e.

the total grain boundary area is large and the degree of internal misorientation is high. In the

as-extruded rod the equiaxed grains and large elongated grains with internal orientation

gradients have mainly a $<10\bar{1}0>$ texture component. As the driving force for grain growth is

consumed within the short annealing time (180 sec annealing under the present conditions),

grain growth is controlled mainly by the preferred growth of grains with the $<11\bar{2}0>$

component such that the corresponding texture component strengthens gradually with

increasing annealing time. After annealing for 1800 sec at 400 °C, the texture transition from

the $<10\bar{1}0>$ into the $<11\bar{2}0>$ component is completed. The gradual disappearance of the large elongated grains with increasing annealing time also contributes to the overall strengthening of the $<11\bar{2}0>$ texture component.

Acknowledgements

References

[1] A. Galiyev, R. Kaibyshev, G. Gottstein, Acta Mater. 49 (2001) 1199.

[2] J.C. Tan, M.J. Tan, Mater. Sci. Eng. A 339 (2003) 124.

[3] S.E. Ion, F.J. Humpreys, S.H. White, Acta Metall. 30 (1982) 1919.

[4] J.A. del Valle, O.A. Runao, Mater. Sci. Eng. A 487 (2008) 473.

[5] M.M. Myshlyaev, H.J. McQueen, A. Mwembela, E. Konopleva, Mater. Sci. Eng. A 337 (2002) 121.

[6] T. Al-Samman, X. Li, S.G. Chowdhury, Mater. Sci. Eng. A 527 (2010) 3450.

[7] S.W. Xu, S. Kamado, N. Matsumoto, T. Honma, Y. Kojima, Mater. Sci. Eng. A 527 (2009) 52.

[8] E. Meza-Garcia, J. Bohlen, D. Letzig, K.U. Kainer, Magnesium Technology, in: R.S. Beals, A.A. Luo, N.R. Neelameggham, M.O. Pekguleryuz (Eds.), TMS, 2007, 263.

[9] H. Ding, L. Liu, S. Kamado, W. Ding, Y. Kojima, J. Alloys Compd. 456 (2008) 400.

[10] S.S. Park, B.S. You, D.J. Yoon, J. Mater. Process. Technol. 209 (2009) 5940.

[11] W.H. Sillekens, J.A.F.M. Schade van Westrum, A.J. den Bakker, P.-J. Vet, Mater. Sci. Forum 426-432 (2003) 629.

[12] S. Ishihara, H. Shibata, K. Komano, T. Goshima, Z.Y. Nan, Key Eng. Mater. 353-358 (2007) 291.

[13] Y. Chen, Q. Wang, J. Peng, C. Zhai, W. Ding, J. Mater. Process. Technol. 182 (2007) 281.

[14] J. Swiostek, J. Göken, D. Letzig, K.U. Kainer, J. Mater. Eng. Perform. 15 (2006) 705.

[15] N. Stanford, D. Atwell, A. Beer, C. Davies, M.R. Barnett, Scripta Mater. 59 (2008) 772.

[16] R.K. Mishra, A.K. Gupta, P.R. Rao, A.K. Sachdev, A.M. Kumar, A.A. Luo, Scripta Mater. 59 (2008) 562.

[17] M. Shahzad, L. Wagner, J. Alloys Compd. 486 (2009) 103.

[18] K.Mueller, S. Mueller, J. Mater. Process. Technol. 187-188 (2007) 775.

[19] M. Paramsothy, S.F. Hassan, N. Srikanth, M. Gupta, J. Alloys Compd. 482 (2009) 73.

[20] T. Laser, Ch. Hartig, M.R. Nürnberg, D. Letzig, R. Bormann, Acta Mater. 56 (2008) 2791.

[21] J. Bohlen, S.B. Yi, J. Swiostek, D. Letzig, H.-G. Brokmeier, K.U. Kainer, Scripta Mater. 53 (2005) 259.

[22] H.-G. Brokmeier, Phys. B 213-214 (1997) 1144.

[23] G. Wassermann, J. Grewen, Texturen metallischer Werkstoffe, Springer-Verlag, Berlin, 1962.

[24] C. Barrett, T.B. Massalski, Structure of Metals, third ed., Pegamon Press, Oxford, 1980.

[25] I.L. Dillamore, P. Hadden, D.J. Stratford, Metall. Rev. 10 (1965) 271.

[26] F.J. Humphreys, M. Hatherly, Recrystallization and related annealing phenomena, Elsevier Ltd., Oxford, 1996.

Fig. 5. Kernel average misorientation maps marked with HAGBs, constructed using the orientation relationship with 3rd neighbours, of (a) the as-extruded bar and (b) the sample annealed for 180 sec at 400 °C (because of the large difference in grain size, different magnifications are used, note the micron-bars). (c) Variation of the area fraction of grains having kernel average misorientations larger than 2 ° during annealing at 400 °C. The grains marked with white circles in (a) correspond to those marked in Fig. 3 (b).

Fig. 6. EBSD orientation maps of the samples annealed for (a) 600 sec and (b) 1800 sec at 400 °C. (c) Inverse pole figure evaluated from the equiaxed grains within the large elongated ones in the sample annealed for 600 sec, as marked with the dashed rectangle in (a) (Levels: 1.0, 1.5 … 3.5 m.r.d.).

Fig. 7. Variation of the (a) size distributions of the equiaxed grains calculated from the EBSD orientation maps and (b) area fractions of the grains with $<10\bar{1}0>$ and $<11\bar{2}0>$ components during annealing at 400 °C. The arrow in Figure (a) shows the rapid decrease in the area fraction of the fine grains smaller than 5 µm.

Fig. 8. Inverse pole figures evaluated from the equiaxed grains larger than 40 µm in the samples annealed for 180 sec, 600 sec and 1800 sec at 400 °C (Levels: 1, 2, 3 … 11 m.r.d.).

Table 1. Variation of the area fractions of equi-axed grains as a function of the annealing time at 400 °C. The area fraction of equi-axed grains with $<10\bar{1}0>$ and $<11\bar{2}0>$ components were calculated with 15 ° of orientation deviation. (*: the numbers in the blanks are the average sizes in µm of the grains with the given orientations)

	As-ext.	180 sec	300 sec	600 sec	900 sec	1800 sec
Grains < 5µm	0.62	0.11	0.05	0.03	0.01	0.01
Grains > 40µm	0	0.19	0.21	0.23	0.23	0.27
Grains with $10\bar{1}0$	0.33 (3.53)	0.16 (15.4)	0.19 (21.4)	0.16 (20.4)	0.12 (21.4)	0.15 (24.1)
Grains with $11\bar{2}0$ *(aver. G.S., µm)*	0.14 (3.89)	0.32 (26.1)	0.33 (27.0)	0.35 (32.9)	0.30 (32.1)	0.40 (38.7)
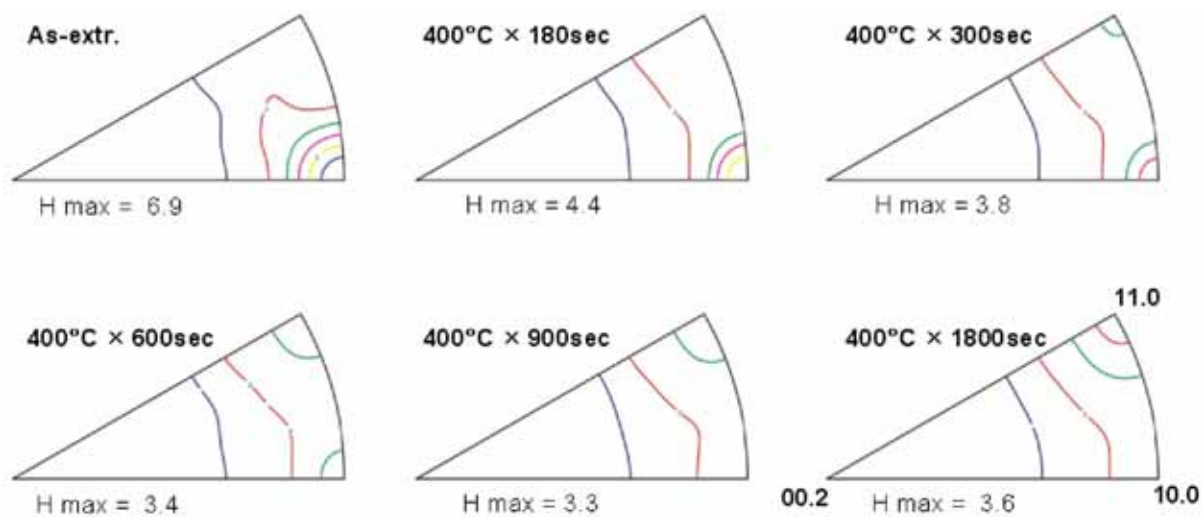
Fig. 1. Inverse pole figures in the ED, measured by neutron diffraction, of the as-extruded bar and after annealing at 400 °C for various holding times (Levels; 1, 2, … 6 multiple random degree, m.r.d.).
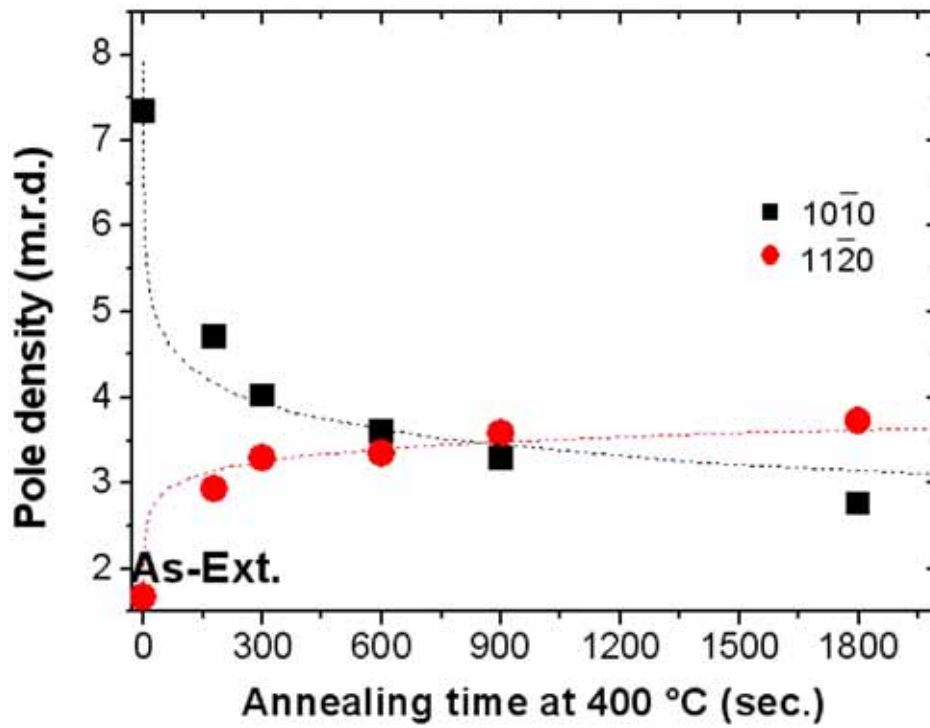
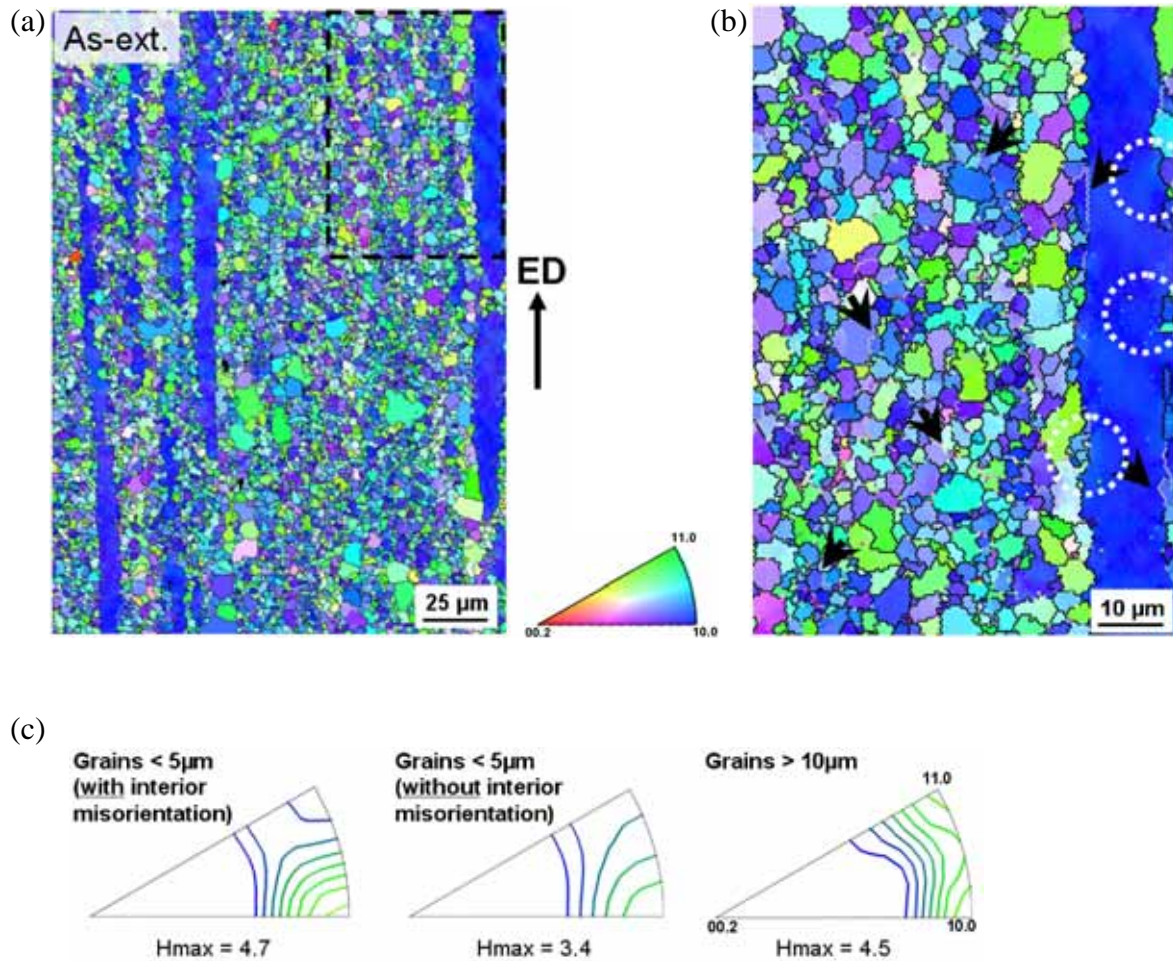Fig. 2. Variation of the $<10\bar{1}0>$ and $<11\bar{2}0>$ pole densities as a function of the annealing time at 400 °C.

Fig. 3. (a) EBSD orientation map of the as-extruded bar, colour code: inverse pole figure in the ED. (b) Magnified view of the marked area in the left figure, for showing the misorientation and new grains formed at grain boundaries. (c) Inverse pole figures evaluated from the equi-axed grains smaller than 5 µm with and without showing the interior misorientations, and from the equi-axed grains larger than 10 µm (Level: 1, 1.5, 2.0 … 4.5 m.r.d.).
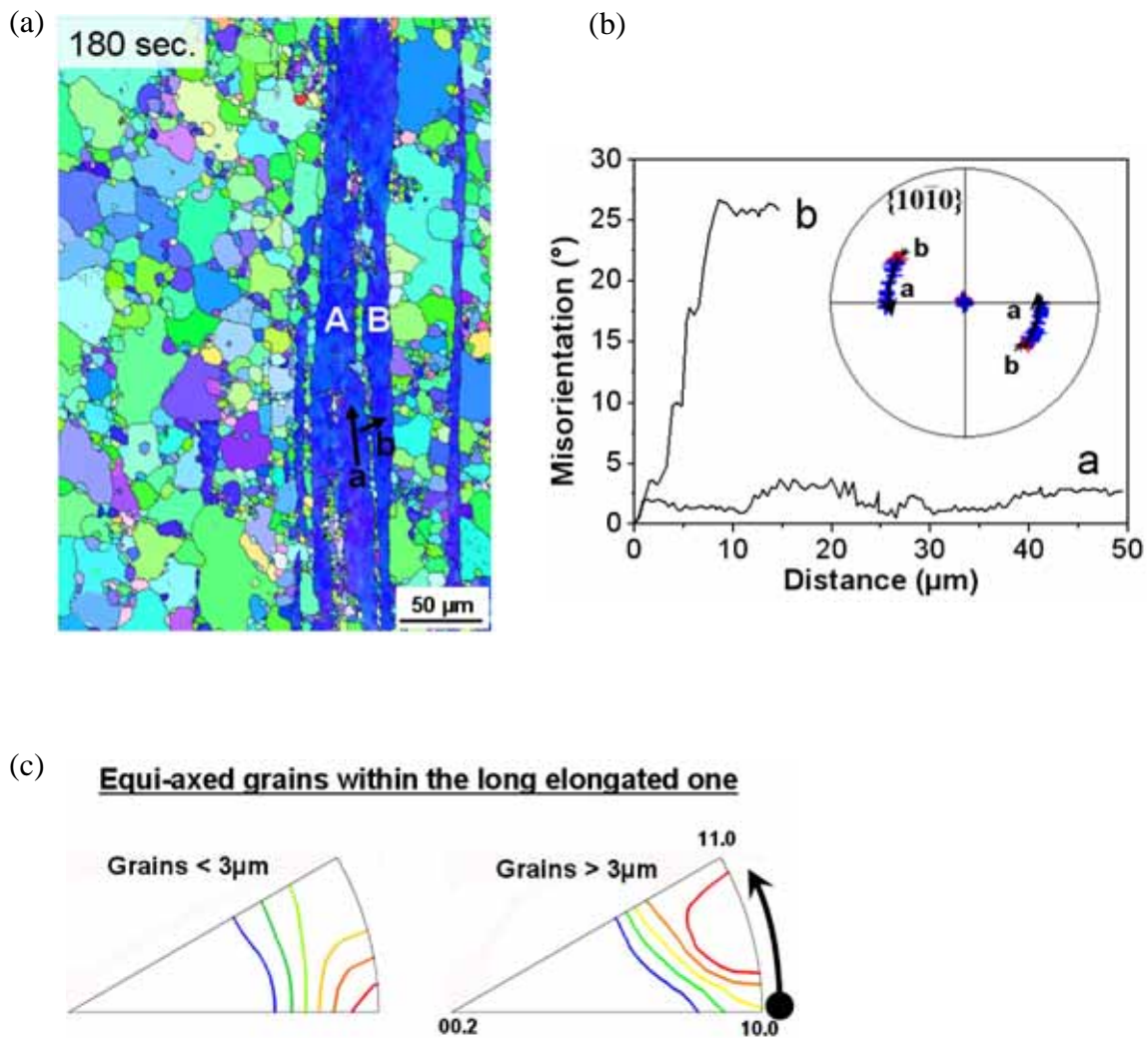
Fig. 4. (a) EBSD orientation map of the 180 sec annealed sample at 400 °C. (b) Misorienation profiles along the arrows 'a' and 'b': the corresponding orientation changes are plotted on the $\{10\bar{1}0\}$ pole figure. (c) Inverse pole figures in the ED taken from equi-axed grains, larger and smaller than 3 μm, existing in the long elongated ones (Levels; 1, 1.5, … 3.0, H_{max} = 4.3 m.r.d.).
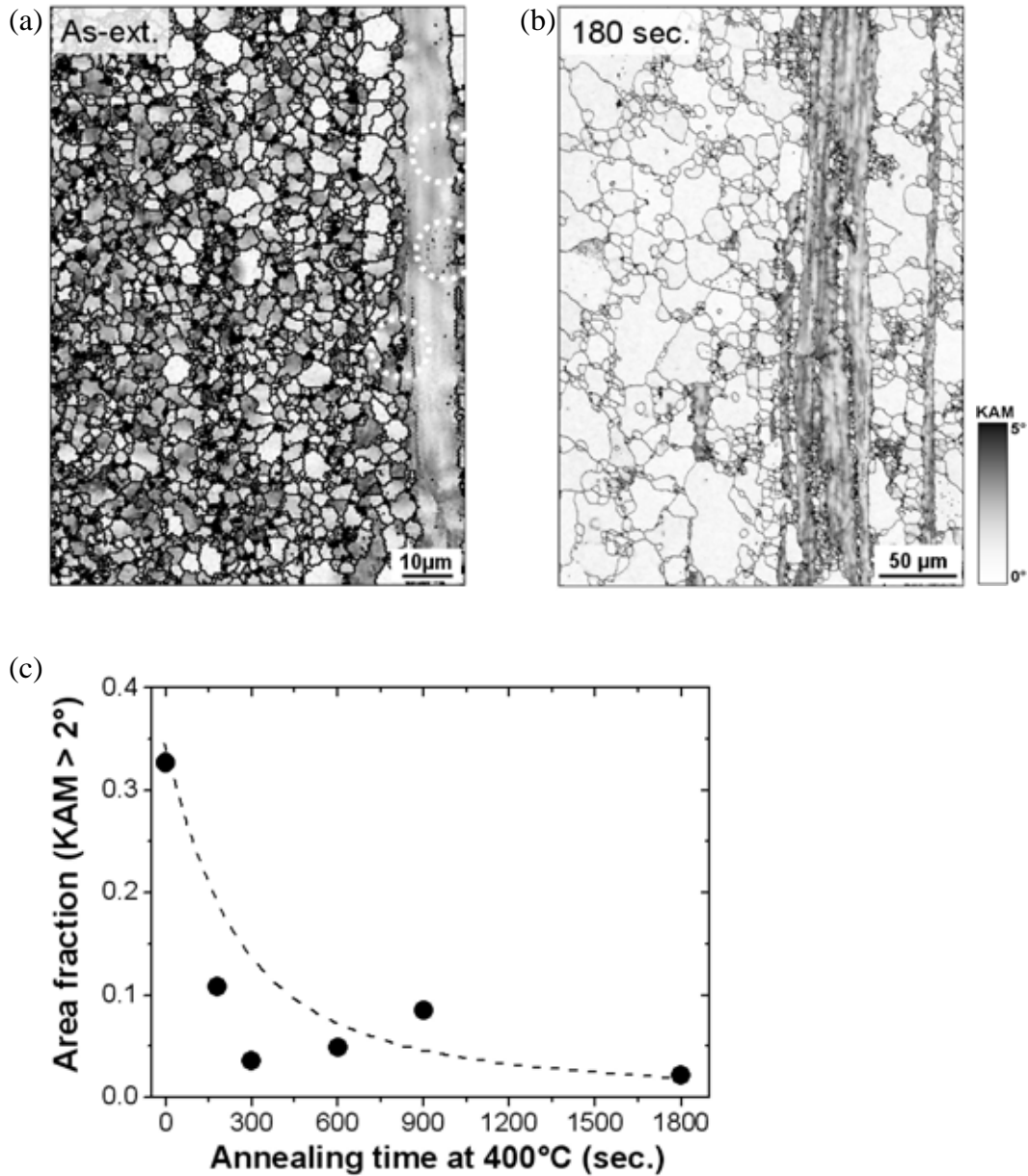
Fig. 5. Kernel average misorientation maps marked with HAGBs, constructed using orientation relationship with 3rd neighbours, of (a) the as-extruded bar and (b) 180 sec annealed samples at 400 °C (because of the large difference in the grain sizes, the different magnifications are applied, refer the micron-bars). (c) Variation of the area fraction of the grains having kernel average misorientation larger than 2 ° during the annealing at 400 °C. The grains marked with white circles in the (a) correspond to those marked in Fig. 3 (b).
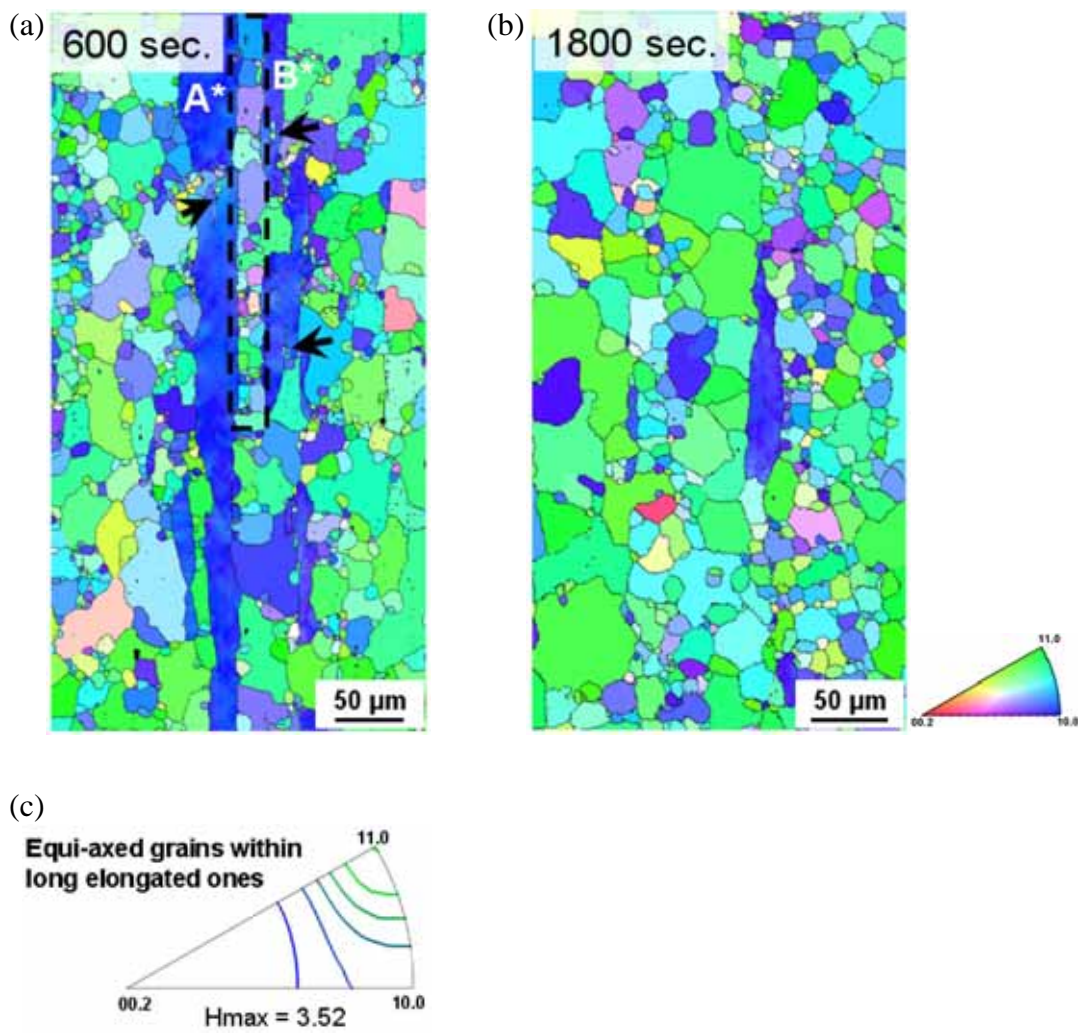
Fig. 6. EBSD orientation maps of the (a) 600 sec and (b) 1800 sec annealed samples at 400 °C. (c) Inverse pole figure evaluated from the equi-axed grains within the long elongated ones in the 600 sec annealed sample, marked with the dashed rectangle in the (a) (Levels: 1.0, 1.5 … 3.5).
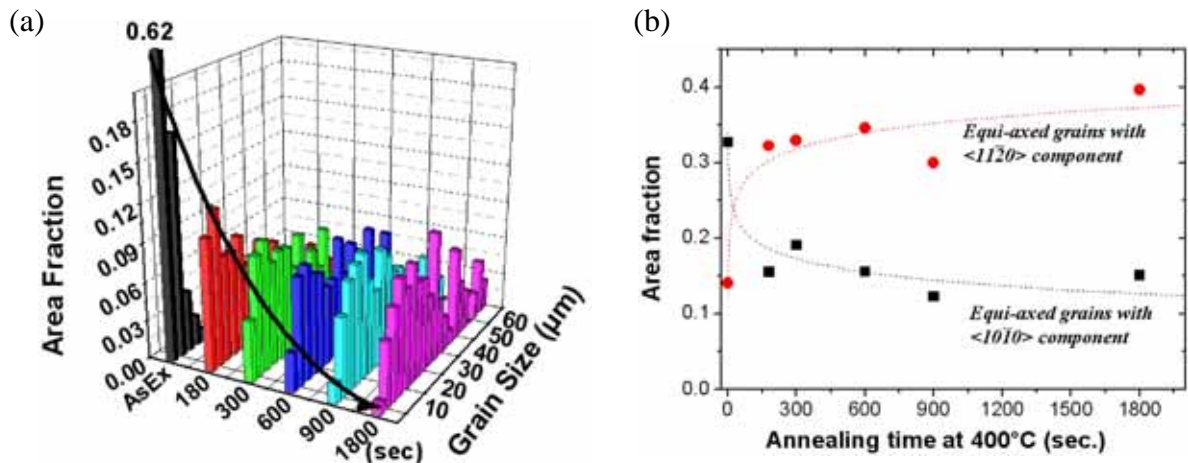
Fig. 7. Variation of the (a) size distributions of the equi-axed grains calculated from the EBSD orientation maps, except the long elongated ones, and (b) area fractions of the grains with $<10\bar{1}0>$ and $<11\bar{2}0>$ components during the annealing at 400 °C. The arrow in figure (a) shows the rapid decrease in the area fraction of the fine grains smaller than 5 µm.
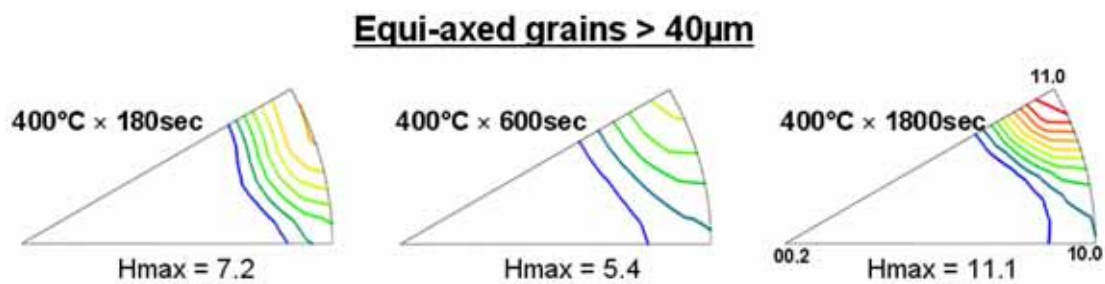
Equi-axed grains > 40μm

400°C × 180sec   Hmax = 7.2

400°C × 600sec   Hmax = 5.4

400°C × 1800sec   Hmax = 11.1

11.0

00.2   10.0

Fig. 8. Inverse pole figures evaluated from the equi-axed grains larger than 40 µm in the samples annealed for 180 sec, 600 sec and 1800 sec at 400 °C (Levels: 1, 2, 3 … 11 m.r.d.).